Beam-Attenuation Measurement Error Due to Small-Angle Scattering Acceptance

KENNETH J. VOSS

Physics Department, University of Miami, Coral Gables, Florida

ROSWELL W. AUSTIN

Center for Hydrologic Optics and Remote Sensing, San Diego State University, San Diego, California

(Manuscript received 18 November 1991, in final form 11 July 1992)

ABSTRACT

Transmissometers always accept a certain portion of the forward-scattered light. The error in the beam-attenuation coefficient $c(\lambda)$ due to this acceptance varies with the small-angle scattering function, single-scattering albedo, and instrumental design. This paper details methods to model error in measurements of $c(\lambda)$ obtained with cylindrically limited and collimated-beam transmissometers. These models are used with real examples of beam attenuation and small-angle scattering function data to test how this measurement error varies.

1. Introduction

The spectral beam-attenuation coefficient $c(\lambda)$ is an important parameter in describing the optical properties of ocean water. The measuring process almost universally involves measurement of the transmittance $T(\lambda)$ of the water over some pathlength R, and then conversion of this transmittance to $c(\lambda)$ $\{c(\lambda) = -\ln[T(\lambda)]/R\}$ in the data reduction process. (A list of symbols is given in the Appendix.) The water transmission is measured by illuminating a volume of water with a well-defined beam of light and then collecting the light that has not been scattered or absorbed after a known distance. Unfortunately, the light scattering by the particulates in seawater is very intense in the forward direction, and a large percentage of light is scattered with small angular deviation. This light should not be included in the "transmitted" light but, to varying degrees, is treated by all transmissometers as part of the unscattered light.

Besides causing a problem in obtaining a correct value for $c(\lambda)$, this sharply peaked light-scattering phase function causes another problem; namely, transmissometers with different optical configurations will differ in the value of $c(\lambda)$ obtained for the same water sample. This makes comparisons of measurements with different transmissometers difficult, and at the least implies that the transmissometer design be specified when $c(\lambda)$ measurements are reported (a practice that is not generally followed). In some applications of the beam-attenuation coefficient a value of $c(\lambda)$ is required that excludes all forward scattering. In this case some methodology must be developed to estimate the error in the transmissometer measurement due to this unwanted small-angle scattered light.

In this paper we will detail methods of correcting measurements of $c(\lambda)$ obtained with two different transmissometer designs, the Alpha and Small Angle Scattering Instrument (ALSCAT) (Austin and Petzold 1975) and the Vislab Spectral Transmissometer (VLST) (Petzold and Austin 1968). These instruments are used as examples, but the same formalism could be extended to other transmissometers of similar designs.

2. Description of the instruments

As mentioned, these two instruments use very different optical designs to obtain the water transmission. The first instrument, ALSCAT, has the traditional collimated-beam design, which is used in this instrument to allow auxiliary measurements of small-angle forward scattering. In ALSCAT, the source field stop is placed at the focal distance of the source objective lens. Thus, the light exiting the source is collimated, with a beam divergence related to the size of the source field stop and the focal length of the source objective lens. The receiver optics is designed to collect the light from the source, with an angular acceptance somewhat larger than the beam divergence of the source. The smaller the source divergence, the smaller the angular acceptance of the receiver can be. In ALSCAT's case, the angular acceptance is 1.5 mrad, or 0.08°. Another transmissometer that uses this design is the Sea Tech transmissometer, with a 1° acceptance angle.

The VLST is a cylindrically limited beam transmis-

Corresponding author address: Kenneth J. Voss, University of Miami, Department of Physics, P.O. Box 248046, Coral Gables, FL 33124-0530.

someter in which the field stop for the source is imaged on the entrance aperture of the receiver objective lens (in air), while the field stop of the receiver is imaged, with the receiver objective lens, on the exit aperture of the source lens (in water). All light is accepted by the receiver if it appears to be coming from the direction of the source lens aperture and hits the receiver objective lens. The advantages of this design are twofold. First, a large volume of water is evenly illuminated; thus, the transmittance obtained is averaged over more water. Second, more of the flux of an extended source is used in the instrument. Both of these factors result in a transmissometer that is well suited to general oceanographic use. The limitation of this design is that it has a maximum angular acceptance on the receiver side, which is the ratio of two times the beam diameter and the beam pathlength. The VLST is a 1-m pathlength transmissometer, with a beam diameter of 2 cm; thus, the maximum acceptance is approximately 2.3°. This angular acceptance varies throughout the illuminated volume, thus complicating correction algorithms. The Martek transmissometer, a commercially available transmissometer, also uses this design. These two transmissometer designs are shown in Fig. 1.

With the transmissometer designs in mind, we progress to determine the measurement error associated with them.

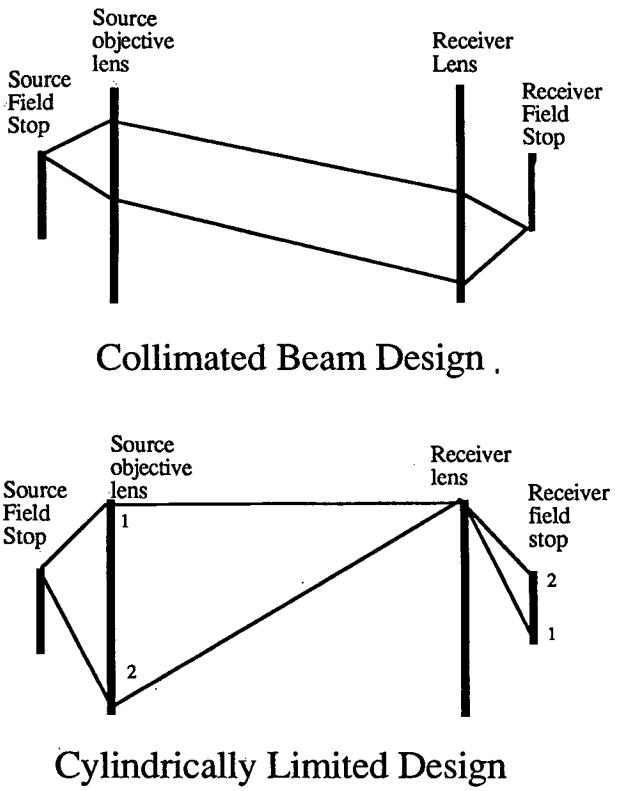

FIG. 1. Ray trace diagram with representative rays for both collimated and cylindrically limited transmissometer designs. In the collimated-beam design, the rays leaving any point on the source field stop will exit the source objective lens parallel to each other. These rays are then imaged by the receiver lens to a point on the receiver field stop. In the cylindrically limited design, a point in the source field stop is imaged to a point on the receiver lens; it is not imaged at the receiver field stop, but rather fills the receiver field stop.

3. Error-estimation algorithms

Correction of the transmittance readings of both transmissometer designs requires knowledge of the small-angle scattering function $\beta(\theta)$, which unfortunately is not measured routinely. Scattering function $\beta(\theta)$ is defined as

$$\beta(\theta) = \frac{dI(\theta)}{E dV},$$

where $I(\theta)$ is the scattered intensity, E is the incident irradiance, and dV is the scattering volume, that is, the volume of sample illuminated by E from which the scattered light is received. ALSCAT provides the small-angle phase function at three angles: 3, 6, and 12 mrad (Austin and Petzold 1975). Data from an instrument of the same optical design has been used extensively in ocean optics literature (Petzold 1972); however, these data do not include information on how the small-angle scattering function may vary with wavelength, and this information was required for our analysis. Fortunately, ALSCAT allows measurement of $\beta(\theta)$ at several different wavelengths. We will use a collection of previously unpublished data from ALSCAT (data shown in Table 1) exclusively in this report.

In this paper we assume that the measurements obtained with ALSCAT are a correct representation of the small-angle portion of the scattering function. Measurements by Spinrad et al. (1978) indicated that the scattering function should be almost constant at small angles. These measurements, however, were performed on monodisperse collections of spheres, not ocean water with its polydisperse assortment of particles. As illustrated in the paper by Spinrad et al., most measurements of seawater (including ALSCAT) are fairly similar and quite different from the monodisperse sphere measurements. Also, we will be using diffraction theory to describe the very small angle scattering. Small-angle scattering is dominated by large particles [diameter larger than the wavelength of light: Hodera (1964)]. While the total scattering coefficient and the large-angle portion of the scattering function (particularly backscattering) may be controlled by small phytoplankton and bacteria, the scattering at angles less than 1° is predominantly due to large particles. This can be seen in Fig. 1 of Spinrad et al. (1978), where the scattering at angles less than 1° is three to four orders of magnitude greater for particles with a diameter of 19.5 μm than at 2 μm. Size-distribution measurements (Gordon et al. 1972) indicate that the decrease in numbers of particles between 2 and

TABLE 1. ALSCAT small-angle scattering function and beam-attenuation values.

Wavelength (nm)	3 mrad (m^{-1} sr^{-1})	6 mrad (m^{-1} sr^{-1})	12 mrad (m^{-1} sr^{-1})	c (m^{-1})
440	2350	1060	420	3.730
	220	90.0	35.0	0.364
	1470	590	215	1.088
	700	300	110	0.844
	320	127	48.0	0.543
	100	44.0	18.0	0.122
	625	320	140	1.082
	157	65.0	27.0	0.301
	150	51.5	18.5	0.201
490	84.0	37.0	15.0	0.118
	580	275	105	0.799
	280	125	43.0	0.491
	145	46.5	15.0	0.180
	2200	980	429	3.244
	190	82.0	32.0	0.333
	1410	570	215	1.024
520	1280	500	200	1.008
	2060	890	375	3.016
	190	80.0	28.0	0.354
	530	260	115	0.968
	127	51.5	22.0	0.278
	82.0	33.0	13.0	0.135
	630	295	110	0.787
	260	120	42.0	0.507
	142	44.0	14.0	0.198
550	260	115	43.0	0.514
	630	290	110	0.777
	76.0	32.0	13.0	0.149
	119	47.5	20.0	0.285
	500	248	110	0.968
	139	41.5	12.5	0.201
	190	80.0	32.0	0.357
	1880	850	370	2.797
	1250	600	210	1.000
670	225	102	37.0	0.798
	130	35.0	9.50	0.531
	94.0	36.5	15.0	0.589
	410	198	90.0	1.214
	60.0	26.0	11.0	0.494
	550	258	110	1.056
	1000	410	170	1.207
	185.0	78.0	32.0	0.677
	1400	660	290	2.564

19.5 μm is not sufficient to offset this difference in scattering. Thus, the small-angle scattering will be due to relatively few large particles. It is also important to note that diffraction theory and Mie scattering theory are not mutually exclusive; diffraction is the small-angle component of Mie scattering theory. By separating diffraction from the general-angle case of Mie scattering theory we can describe the small-angle portion of the scattering function in a simplified manner.

In the case of a collimated-beam transmissometer, correction for forward-angle acceptance is relatively straightforward once $\beta(\theta)$ is known. In this case, one can separate the measured beam-attenuation coefficient into its component constituents (the wavelength dependence of these factors will not be shown explicitly in the following discussion):

$$c = b + a,$$

where b is the total scattering coefficient and a is the total absorption coefficient. The total scattering coefficient is defined as

$$b = 2\pi \int_0^{\pi} \beta(\theta) \sin(\theta) d\theta,$$

where θ is the scattering angle. At this point b can be further separated into two components: a small-angle component and the remainder of the scattering coefficient. Thus,

$$b_{\text{total}} = b_{\text{small}} + b_{\text{large}}$$

$$b_{\text{small}} = 2\pi \int_0^{\theta_0} \beta(\theta) \sin(\theta) d\theta$$

$$b_{\text{large}} = 2\pi \int_{\theta_0}^{\pi} \beta(\theta) \sin(\theta) d\theta,$$

with θ_0 defined by the angular acceptance of the transmissometer receiver optics. Thus, the collimated transmissometer measures

$$c_{\text{measured}} = c_{\text{true}} - b_{\text{small}},$$

and the correction is

$$c_{\text{true}} = c_{\text{measured}} + b_{\text{small}}.$$

If $\beta(\theta)$ is known, c_{true} can be determined. If $\beta(\theta)$ is not known but varies in some regular manner with c, then from an archive of $\beta(\theta)$ and c measurements, c_{true} can be approximated.

ALSCAT measures $\beta(\theta)$ down to 3 mrad, but if we are to model the beam-attenuation measurement of ALSCAT, we need to know $\beta(\theta)$ from 0 to 1.5 mrad (the acceptance angles of ALSCAT). As explained earlier, we believe the best method to extrapolate $\beta(\theta)$ is a model based on diffraction theory, since the small-angle scattering is dominated by diffraction. Our model is based on this assumption and that of spherical particles.

Van de Hulst (1981) gives the formulation of the diffraction pattern from a target as

$$E(\theta) = \frac{G^2}{\lambda^2 r^2} E_o |D(\theta, \phi)|^2.$$

Where E is the scattered radiant intensity, E_o is the incident irradiance, D is the amplitude of the diffraction pattern, G is the geometric projected area of the particle, and r is the distance to the measuring point. In the specific case of a sphere, $G = \pi\rho^2$, where ρ is the radius of the sphere,

$$x = \frac{2\pi\rho}{\lambda}, \quad D = \frac{2J_1(x \sin\theta)}{x \sin\theta},$$

where J_1 is the first-order Bessel function. Therefore,

$$E(\theta) = \frac{\rho^2}{r^2} E_o \left| \frac{J_1(x \sin\theta)}{\sin\theta} \right|^2$$

and $$\beta(\theta) = \frac{E(\theta) r^2}{V E_o} = \frac{\rho^2}{V} \left| \frac{J_1(x \sin\theta)}{\sin\theta} \right|^2.$$

For a collection of particulates, arranged randomly, the scattering will add incoherently; thus,

$$\beta(\theta) = \sum_{\rho=0}^{\rho_{\max}} F(\rho) \rho^2 \left| \frac{J_1(x \sin\theta)}{\sin\theta} \right|^2,$$

where $F(\rho)$ is the particle-size distribution of the collection of particles. In this model, $F(\rho)$ is chosen to be a Junge distribution $F(\rho) = A\rho^{-m}$, so

$$\beta(\theta) = \sum_{\rho=0}^{\rho_{\max}} A\rho^{2-m} \left| \frac{J_1(x \sin\theta)}{\sin\theta} \right|^2.$$

In fitting this to the data one needs to determine m, A, and $\rho_{\max}$. Morel (1973) found the exponent of the size distribution, m, varied by the slope w of $\log\beta(\theta)$ versus $\log\theta$ at small angles as $m = w + 5$. The small angle (0.1°–1°) portion of the scattering function also appears linear on a plot of $\log\theta$ versus $\log\beta(\theta)$; thus, $\beta(\theta)$ can be described in this region as

$$\beta(\theta) = K\theta^w.$$

The limits of the summation can be determined by looking at $d\beta(\theta)/d\theta$, as given by diffraction theory and $d\beta(\theta)/d\theta$ for the small-angle data. The quantity $d\beta(\theta)/d\theta$ for the data can be found by differentiating the preceding form for $\beta(\theta)$; that is,

$$\frac{d\beta(\theta)}{d\theta} = \frac{Kw\theta^w}{\theta} = \frac{w\beta(\theta)}{\theta}$$

$$w = \frac{\theta}{\beta(\theta)} \frac{d\beta(\theta)}{d\theta}.$$

The diffraction theory expression for $d\beta(\theta)/d\theta$ is

$$\frac{d\beta(\theta)}{d\theta} = \sum_{\rho=0}^{\rho_{\max}} A\rho^{2-m} \frac{d}{d\theta} \left| \frac{J_1(x \sin\theta)}{\sin\theta} \right|^2.$$

Using the small-angle approximation and a simple substitution,

$$\sin\theta = \theta, \quad \phi = x\theta, \quad \text{and} \quad d\phi = x d\theta$$

$$\frac{d\beta(\theta)}{d\theta} = \sum_{\rho=0}^{\rho_{\max}} A\rho^{2-m} x^3 \frac{d}{d\phi} \left| \frac{J_1(\phi)}{\phi} \right|^2$$

$$= \sum_{\rho=0}^{\rho_{\max}} A\rho^{2-m} x^3 \left(\frac{2J_1 J_0}{\phi^2} - \frac{4J_1^2}{\phi^3} \right).$$

Therefore,

$$w = \frac{\theta}{\beta(\theta)} \frac{d\beta(\theta)}{d\theta} = \frac{\sum_{\rho=0}^{\rho_{\max}} \rho^{2-m} [2xJ_1J_0 - (4J_1^2/\theta)]/\theta}{\sum_{\rho=0}^{\rho_{\max}} \rho^{2-m} J_1^2/\theta^2};$$

$$= 2 \frac{\sum_{\rho=0}^{\rho_{\max}} \rho^{2-m} \theta x J_1 J_0}{\sum_{\rho=0}^{\rho_{\max}} \rho^{2-m} J_1^2} - 4,$$

and $$\frac{w+4}{2} = \frac{\sum_{\rho=0}^{\rho_{\max}} \rho^{2-m} \theta x J_1 J_0}{\sum_{\rho=0}^{\rho_{\max}} \rho^{2-m} J_1^2}.$$

The upper limit of the summation is determined numerically by comparing the left and right sides of the equation and terminating the summation at the correct $\rho_{\max}$ for equality. At this point, one has $\rho_{\max}$ and m and needs only A, which is found by fitting the equation at the three measured values of $\beta(\theta)$. To determine the small-angle scattering component included in c_{ALSCAT}, one has to integrate this equation from 0 to 1.5 mrad to determine b_{small}:

$$b_{\text{small}} = \int_0^{1.5} 2\pi\beta(\theta)\theta d\theta$$

$$b_{\text{small}} = 2\pi \sum_{\rho=0}^{\rho_{\max}} A\rho^{2-m} \left[\frac{1}{2} - \frac{J_1^2(1.5x)}{2} - \frac{J_2^2(1.5x)}{2} \right].$$

The results of these calculations with measured $\beta(\theta)$'s will be shown in the next section.

The case of the cylindrically limited design is much more complicated because the effective acceptance angle of the receiver depends on the position of the light ray along the axis of the optics, the radial position off-axis, and the initial direction of the light ray. The correction algorithms become more complicated and also contain more approximations. The theory for an analytic correction was first developed by Preisendorfer (1958). In this derivation, however, the assumption was made that the $\beta(\theta)$ was constant at small angles. Our method modifies this formulation to include angular variations in $\beta(\theta)$.

To briefly review his equations, the radiative transfer in the transmissometer is described by the equation

$$\frac{dL'(r', \mathbf{v})}{dr'} = -c'(r')L'(r', \mathbf{v}) + L'(r', \mathbf{v}) \int_{\Sigma_{p(r')}} \beta(r', \mathbf{v}, \mathbf{v}') d\Omega(\mathbf{v}') + \int_{\Sigma - \Sigma_{p(r')}} L(r', \mathbf{v}')\beta(r', \mathbf{v}', \mathbf{v}) d\Omega(\mathbf{v}'),$$

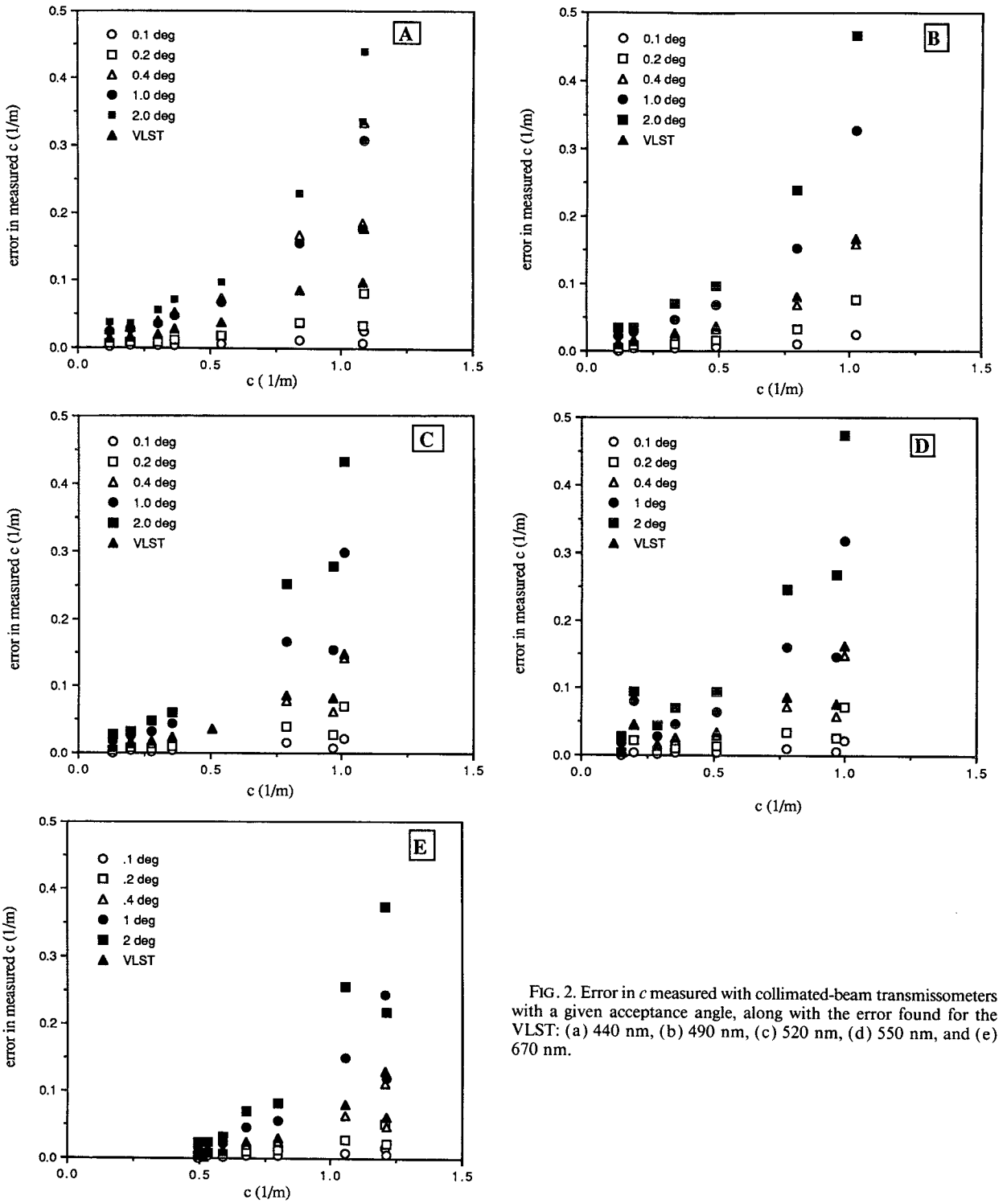

FIG. 2. Error in c measured with collimated-beam transmissometers with a given acceptance angle, along with the error found for the VLST: (a) 440 nm, (b) 490 nm, (c) 520 nm, (d) 550 nm, and (e) 670 nm.

where L' is the radiance due to the transmissometer projector, L is the ambient radiance field, $\Sigma_{p(r')}$ is the solid angle of the receiver, v is the original direction of the light, v′ is any other angle, and Σ is the collection of all angles, that is, the total solid angle is 4π. In this equation the first term on the right is the projector radiance attenuated by scattering and absorption. The second term is the source radiance, which is forward

scattered and still makes it into the receiver, and the third term is ambient light, which is scattered into the receiver. In a well-designed transmissometer, the path radiance (the third term) is equal to zero, so the error in the transmissometer is given by the second term. Preisendorfer sets $\beta(\theta)$ equal to a constant, and it is here we diverge from his derivation.

Let

$$\delta = \int_{\Sigma_{p(r')}} \beta(r', \mathbf{v}, \mathbf{v}')d\Omega(\mathbf{v}') .$$

Integrating δ over the pathlength in the transmissometer, one obtains the result that

$$\frac{L'(r')}{L'(0)} = \exp\left(-cr' + \int_0^{r'} \delta dr''\right).$$

In the cylindrically limited design and for coaxial light rays, $\Sigma_{p(r'')}$ is

$$0 < r'' < R/2; \quad \Sigma_{p(r'')} = \frac{\pi D^2}{4(R - r'')^2}$$

$$R/2 < r'' < R; \quad \Sigma_{p(r'')} = \frac{\pi D^2}{4(r'')^2},$$

where R is the total pathlength of the transmissometer and D is the diameter of the transmissometer. In this way the correction term in the integral is equal to

$$\int_0^{r'} \delta dr'' = \int_0^{R/2} \int_0^{\pi D^2/4(R-r'')^2} \beta(\mathbf{v}', \mathbf{v})d\Omega(\mathbf{v})dr''$$

$$+ \int_{R/2}^{R} \int_0^{\pi D^2/4(r'')^2} \beta(\mathbf{v}', \mathbf{v})d\Omega(\mathbf{v})dr''.$$

Let $R - r'' = r'''$ in the first integral, and $r'' = r'''$ in the second integral, then both integrals become the same and

$$\int_0^{r'} \delta dr'' = 2\int_{R/2}^{R} \int_0^{\pi D^2/4(r''')^2} \beta(\mathbf{v}', \mathbf{v})d\Omega(\mathbf{v})dr'''$$

$$= 2\int_{R/2}^{R} 2\pi \int_0^{D/2(r''')} \beta(\theta)\theta d\theta dr'''.$$

If we assume that the light scattered to less than 1.5 mrad is negligible (we will test this assumption later), then we can change the lower limit of the above integral from 0 to 1.5 mrad. This is useful as it allows us to avoid extrapolating an analytic fit of $\beta(\theta)$ to zero.

In the range of the preceding integrals, $\beta(\theta)$ can be approximated and fit to a function of the form

$$\beta(\theta) = A\frac{e^{-B\theta}}{\theta}.$$

Between 1.5° and 2.3°, there is no significant difference between this function and the function used previously [$\beta(\theta) = K\theta^w$], and this function is much easier to integrate. In this case one has

$$\int_0^{r'} \delta dr'' = \frac{4\pi A}{BR} - \frac{4\pi A}{BR}\int_{R/2}^{R} e^{-B_D/2r'''} dr'''.$$

The second term on the right can be expanded in a power series, and each term integrated individually. In the following calculations, the expansion was terminated when the newest term was less than 1% of the summed expansion to that point. This semianalytical formulation assumes that the initial ray is starting on a coaxial path and is thus an approximation.

We also developed a Monte Carlo–type calculation to model the cylindrically limited system including off-axis paths. This is useful in describing an "exact" solution and in verifying the above semianalytic approximation. This technique consists of tracing the optical light rays through the system, including scattering and absorption in the water path. Many individual photons are followed through the system, and statistics are kept as to the number of rays that have been scattered but still accepted into the receiver optics. In this model, light rays are started along all the possible ray paths in the transmissometer, not just the coaxial path. Thus, this will be a more accurate representation of the transmissometer.

4. Model results

Comparisons of the two techniques for estimation of error in VLST data were run using historical data obtained with ALSCAT. ALSCAT provided the forward-scattering function at three angles and the attenuation coefficient, all at ten wavelengths. Tests cases were run at wavelengths that were close to VLST wavelengths (namely, 440, 490, 520, 550, and 670 nm).

First, the error in c_{ALSCAT} (b_{small}) was tested with the existing ALSCAT dataset, and the results are displayed in Figs. 2a–e. (Note: ALSCAT has an acceptance angle of 0.1°.) The average error is very small for these measurements (on the order of 1%), and thus of negligible importance, and can be neglected in most cases.

This analysis was also carried out for transmissometers with different forward angles of acceptance. To

TABLE 2. Average error for varied angular acceptance for a collimated-beam transmissometer along with error found for the VLST.

Angular acceptance	440 nm	490 nm	520 nm	550 nm	670 nm
0.1°	0.0102	0.0107	0.112	0.0109	0.00976
0.2°	0.0347	0.0365	0.0373	0.0361	0.0349
0.4°	0.1657	0.0790	0.0790	0.0781	0.0771
1.0°	0.155	0.187	0.182	0.187	0.189
2.0°	0.250	0.314	0.292	0.320	0.333
VLST	0.071	0.086	0.084	0.091	0.092

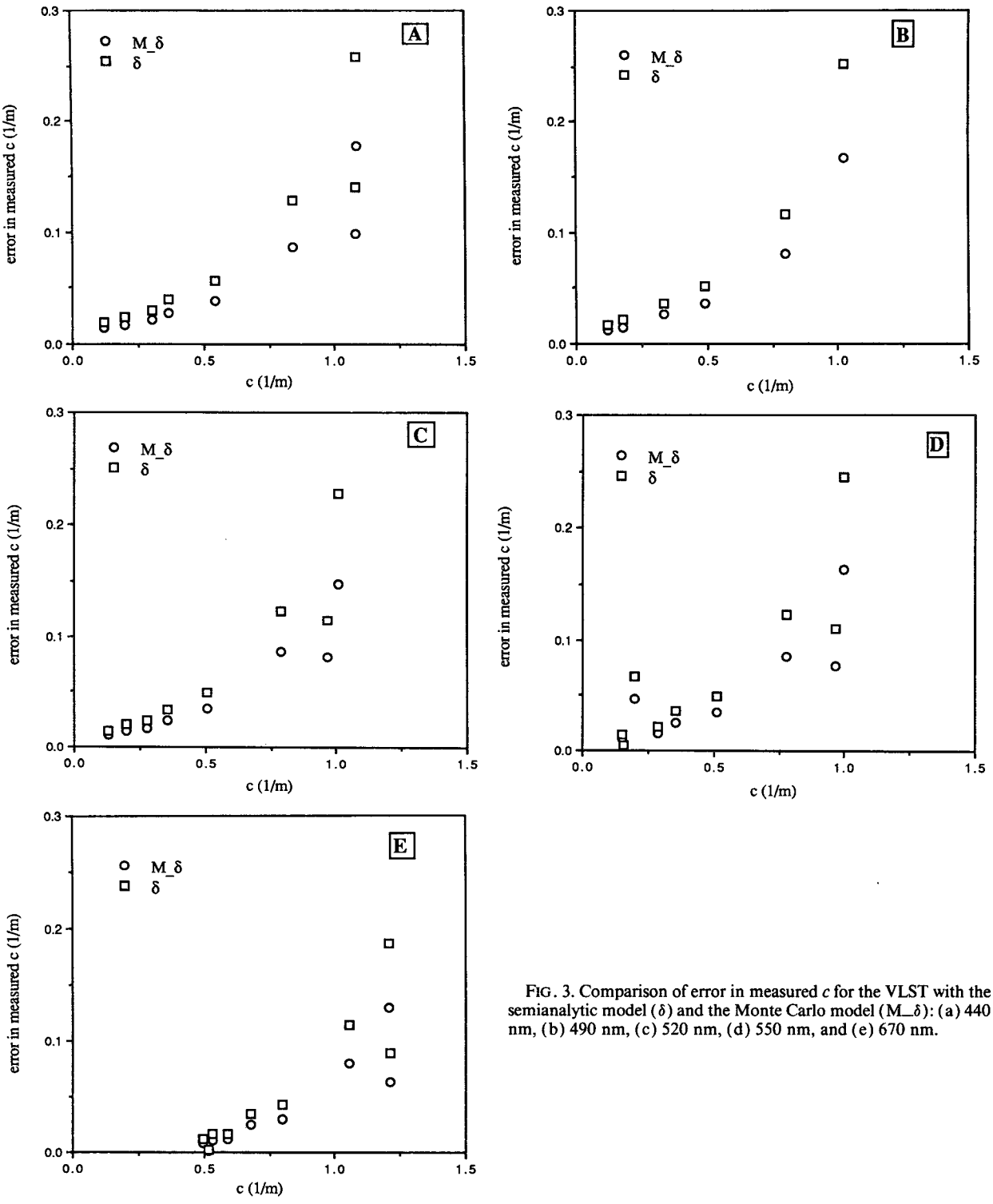

FIG. 3. Comparison of error in measured c for the VLST with the semianalytic model (δ) and the Monte Carlo model (M_δ): (a) 440 nm, (b) 490 nm, (c) 520 nm, (d) 550 nm, and (e) 670 nm.

do this we integrated the analytical fit to the scattering function given previously over the range from 0.1° to the angular acceptance; then we added this portion of b to that found for ALSCAT. The results are also shown in Figs. 2a–e. As can be seen, large errors can result with acceptance angles of only 2°. Average percent errors for each wavelength and angular acceptance were determined by fitting a line to these graphs. The re-

sults are shown in Table 2. Note the SeaTech transmissometer's angular acceptance is 1°.

Calculations were first performed for the VLST using the Monte Carlo simulation but constraining the initial path of the photons along the axis of the transmissometer. These calculations were then compared with results from the semianalytic model. This constrained Monte Carlo model is a direct analog of the semianalytic case, so the errors obtained in each case should be equivalent. It was found that they agree with a maximum deviation of 11% (for 670 nm). Because this was not the major desired result of the Monte Carlo modeling, only 1000 photon "lifetimes" were followed; thus, the results will include noise due to statistical variations. Overall, however, this does confirm that the semianalytic model is calculating the desired function, that is, the error for photons starting out coaxially.

Figures 3a–e illustrate the comparison of the predicted difference between the VLST and ALSCAT measured c's using the semianalytic model (δ) and the Monte Carlo model (M_δ) including off-axis rays. In all cases the Monte Carlo model predicted less error in the c measured with the VLST (i.e., M_$\delta < \delta$). This is due to the dispersion in the initial optical paths of the light rays in the Monte Carlo case. As stated earlier, in the semianalytic case, the light rays were all considered to have started going down the center of the transmissometer. One can think of the probability of having scattered photons accepted as a convolution of the solid angle of acceptance with the scattering phase function. As one moves off the central ray, the solid angle of acceptance is no longer centered on the sharply peaked phase function, and the probability of scattering still being accepted is smaller (the convolution is reduced). Basically, the semianalytic approximation seems to overestimate the error by a factor of 1.6.

As an aside, we have shown the M_δ in Figs. 2a–e and the average percent difference in Table 2 (as VLST). Even though this transmissometer design has a large maximum acceptance angle, the error is equivalent to a collimated transmissometer with a forward angle of acceptance of 0.4°.

The data in Table 2 could be used to correct collimated-beam transmissometers for the small-angle scattering error; however, factors such as variance in the single-scattering albedo ω and variations in the particle-size distribution (which changes the slope of the small-angle scattering function) can interfere with this scheme. An illustration of the variation is shown in Figs. 2a, 2c–e, 3a, and 3c–e. At all of these wavelengths the two highest values of the beam attenuation are very similar, but the small-angle portion of the scattering function for these points varied by almost a factor of 2. There is no technique to separate effects due to changes in the particle size distribution from changes in ω without auxiliary measurements. These data points, however, illustrate the range of variation that can occur. To get more accurate corrections for specific cases the small-angle scattering function must be known.

All of these graphs also illustrate that as the beam attenuation gets larger, the percentage error grows. There are several effects occurring that can cause this. The first is that in very clear water the beam attenuation is dominated by the beam attenuation of the water. The beam attenuation of the water is predominantly due to absorption, and the scattering that occurs is mainly large-angle scattering. Both of these factors cause no error in the measured c. As the water gets more turbid, the particulate component of the beam attenuation grows; thus, the small angle $\beta(\theta)$ increases faster than c. This increase in $\beta(\theta)$ causes the error in measured c to grow at a rate faster than c; hence, the percent error in c increases. The range of beam attenuation in the ocean however is limited, for the most part, to values less than 1. Only in intense blooms (see, for example, Balch et al. 1991) or turbid harbor or estuary conditions does c (490 nm) reach values significantly above 1. In the turbid water conditions, multiple-scattering effects will cause significant errors in beam-attenuation measurements with a 1-m pathlength transmissometer. Additional causes for the increasing percent error can be varying particle-size distribution and ω as c increases, but we did not have auxiliary measurements that could have isolated these effects.

In conclusion, we have shown two methods for predicting the error in c_{VLST} and c_{ALSCAT}. The errors predicted with these techniques appear to follow a regular pattern; however, changes in b/c and the small-angle scattering function can cause variations in the percent error. These analysis methods can also be extended to analysis of other transmissometer designs.

Acknowledgments. We would like to acknowledge the generous support of the Ocean Optics division of the Office of Naval Research and the Applied Physics Laboratory, Johns Hopkins University.

APPENDIX

List of Symbols

Symbol	Definition	Units
a	Total absorption coefficient	m^{-1}
b	Total scattering coefficient	m^{-1}

b_{small}	Small-angle component of scattering coefficient	m^{-1}
$\beta(\theta)$	Scattering function	m^{-1} sr^{-1}
$c(\lambda)$	Spectral beam attenuation	m^{-1}
E	Irradiance	μW cm^{-2} nm^{-1}
$F(\rho)$	Size distribution of particles	number per cubic meter
G	Geometric cross section of particles	m^2
$I(\theta)$	Scattered radiant intensity	μW sr^{-1}
J_1	First-order Bessel function	
L	Radiance	μW cm^{-2} nm^{-1} sr^{-1}
λ	Wavelength	nm
m	Exponent in the Junge size distribution	
R	Pathlength of transmissometer	m
ρ	Radius of particle	m
Σ	Solid angle	sr
$T(\lambda)$	Spectral transmission	dimensionless
θ	Angle	radians or degrees
$\mathbf{v}$	Direction of light ray in transmissometer model	
V	Scattering volume	m^3
w	Slope of $\log[\beta(\theta)]$ versus $\log\theta$	
x	Size parameter of particle = $2\pi\rho/\lambda$	dimensionless

REFERENCES

Austin, R. W., and T. J. Petzold, 1975: An instrument for the measurement of spectral attenuation coefficient and narrow angle volume scattering function of ocean waters. *Ocean Opt.*, **64**, 50–61.

Balch, W. M., P. M. Holligan, S. G. Ackleson, and K. J. Voss, 1991: Biological and optical properties of mesoscale coccolithophore blooms in the Gulf of Maine. *Limnol. Oceanogr.*, **36**, 629–643.

Gordon, H., H. Bader, and O. Brown, 1972: An experimental and theoretical study of suspended particulate matter in the tongue of the ocean and its influence on underwater visibility. University of Miami, Department of Physics, Final Report, Contract F08606-71-C-0028, 32 pp.

Hodara, H., 1973: Experimental results of small angle scattering. *Optics of the Sea (Interface and in-water transmission and imaging)*. NATO, 17 pp.

Morel, A., 1973: Diffusion De La Lumiere Par Les Eaux de Mer. Resultats experimentaux et approche theorique. *Optics of the Sea (Interface and in-water transmission and imaging)*. NATO, 76 pp.

Petzold, T. J., and R. W. Austin, 1968: An underwater transmissometer for ocean survey work. *Underwater Photo-optical Instrument Applications. SPIE*, **12**, 133–137.

Preisendorfer, R. W., 1958: A general theory of perturbed light fields, with applications to forward scattering effects in beam transmittance measurements. SIO Reference 58–37.

Spinrad, R. W., J. R. V. Zaneveld, and H. Pak, 1978: Volume scattering function of suspended particulate matter at near-forward angles: A comparison of experimental and theoretical values. *Appl. Opt.*, **17**, 1125–1130.

Van de Hulst, H. C., 1981: *Light Scattering From Small Particles.* Dover, 470 pp.